




RESEARCH ARTICLE | AUGUST 23 2024

The role of band-tail states on the electric properties of amorphous chalcogenides: A simulative approach

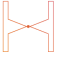
Special Collection: [Phase-change Materials and Their Applications](#)


R. Brunetti ; C. Jacoboni ; M. Rudan 


 Check for updates


J. Appl. Phys. 136, 085701 (2024)
<https://doi.org/10.1063/5.0220117>




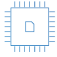
 Nanotechnology & Materials Science

 Optics & Photonics

 Impedance Analysis

 Scanning Probe Microscopy

 Sensors

 Failure Analysis & Semiconductors

The role of band-tail states on the electric properties of amorphous chalcogenides: A simulative approach

Cite as: J. Appl. Phys. **136**, 085701 (2024); doi: [10.1063/5.0220117](https://doi.org/10.1063/5.0220117)

Submitted: 22 May 2024 · Accepted: 7 August 2024 ·

Published Online: 23 August 2024



R. Brunetti,^{1,a)}  C. Jacoboni,¹  and M. Rudan^{2,b)} 

AFFILIATIONS

¹FIM Department, University of Modena and Reggio Emilia, Via Campi 213/A, I-41125 Modena, Italy

²DEI Department, University of Bologna, Viale Risorgimento 2, I-40136 Bologna, Italy

Note: This paper is part of the special topic, Phase-change Materials and Their Applications.

^{a)} **Author to whom correspondence should be addressed:** rossella.brunetti@unimore.it

^{b)} **Also at:** E. De Castro Advanced Research Center on Electronic Systems, University of Bologna, Bologna, Italy.

ABSTRACT

Band-tail states, i.e., charge-carrier energy states located in the bandgap at the valence and conduction band edges of amorphous materials, even though not delocalized, exhibit nonzero mobility; thus, they are expected to contribute to the charge-conduction process. A microscopic model based on hydrodynamic transport equations for unipolar conduction, including trap, band-tail, and band states, and coupled to the Poisson equation is presented here. The equations are self-consistently solved by means of a numerical procedure, and the results provide qualitative and quantitative estimates of the influence of band-tail states (namely, of their energy distribution, density, and mobility) on the carrier heating, precursor of the Ovonic threshold switch.

© 2024 Author(s). All article content, except where otherwise noted, is licensed under a Creative Commons Attribution (CC BY) license (<https://creativecommons.org/licenses/by/4.0/>). <https://doi.org/10.1063/5.0220117>

I. INTRODUCTION

Amorphous semiconductors are variously employed in the design of a wide range of nano-devices. Chalcogenide alloys, in particular, in their both crystalline and amorphous phase, are presently used to design non-conventional electrical and optical memory devices.¹ Such alloys [e.g., GeTe, Ge₂Sb₂Te₅, ZnTe, AgInSbTe (AIST)], which exhibit semiconductor properties, are chemical compounds consisting of at least one chalcogen atom (S, Se, or Te) and one or more electropositive elements. Some of these alloys are made appealing by the possibility to realize a fast and reversible structural switch of the material between the amorphous and crystalline states upon the application of an electric pulse²; in particular, a voltage pulse of suitable intensity and width of a few ns produce an off-to-on threshold switching in the $I(V)$ characteristic of the amorphous state, precursor of the amorphous-to-crystalline phase change. This effect is called *Ovonic Threshold Switching* (OTS; so called because the first investigations were carried out in 1968 by S. Ovshinsky³). Due to this phenomenon, the resistivity of

the material changes by two orders of magnitude at least. The transition between the amorphous and crystalline phases can be controlled by heating (laser irradiation or Joule effect); it is fast (down to few ns⁴), reversible, stable, and has a large duty cycle. Altogether, these properties yield a two-state system able to store logic information.⁵

In amorphous, disordered semiconductors, the energy gap is usually larger than that of crystals. Furthermore, optical-absorption measurements evidence the presence of absorption tails near the optical-band edge. Early measurements reported an exponential tail in the density of states,^{6,7} originally called *Urbach tail*; since then, the presence of weakly localized states in the energy gap has been confirmed by many authors. The physical origin of these tails is still controversial; some authors explain them with reference to the spatial fluctuation of the bond energy, which leads to a broadening of the edges of the conduction and valence bands and introduces energy levels associated to partially localized states.¹ However, no matter what the description of their origin is, what makes these

20 September 2024, 09:29:02

states relevant for transport analysis is the fact that, although not totally delocalised as band states, they have a non-zero (hopping) mobility and are expected to contribute to the transport process.

Besides the above, structural defects introduce energy levels deep in the bandgap region associated with fully localized states, usually referred to as *trap states*.

Due to the presence of band-tail states, the energy interval that separates electron and hole conductive states is smaller than the energy gap of the crystalline material. The effect is sketched in Fig. 1. Carrier-energy spectrum and DOS of amorphous chalcogenides are obviously relevant for charge-transport analysis. Unfortunately, in many cases, experimental information and atomistic calculations are not accurate enough to provide reliable grounds for a transport theory. Atomistic simulations are indeed very challenging: they require large cells and a huge number of atoms, resulting in heavy computational loads;⁸ although calculations exhibit a qualitative agreement with experiments, neither one is able to provide reliable data for transport analysis. As a consequence, some features must be modeled with the introduction of parameters, to be determined by the comparison with transport and optical data for the chalcogenide in hand.

The OTS effect has extensively been studied, both experimentally and theoretically, by means of numerical simulations including trap states and mobile band states with parabolic dispersion;^{9,10} unipolar conduction is usually assumed although, recently, impact ionization has been proposed as the responsible mechanism for negative differential resistance in materials with bipolar conduction exhibiting a strong unbalance between hole and electron mobilities.¹¹

The approach adopted in the past by the authors of this paper is based upon a unipolar conduction model. By numerically solving

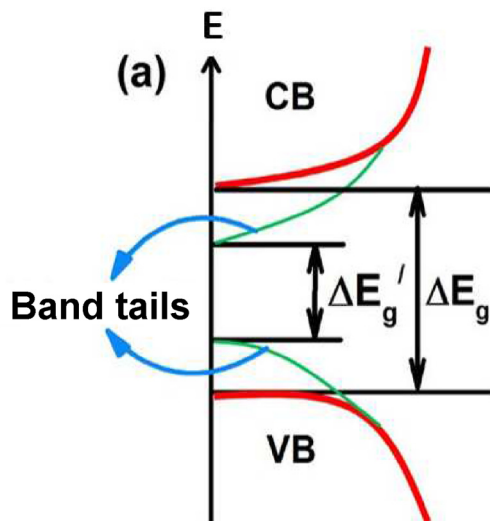


FIG. 1. Qualitative description of the band-tail states. Due to their presence, the energy interval $\Delta E'_g$ that separates electron and hole conductive states is smaller than the energy gap ΔE_g of the crystalline material (the actual band structure of the material used in the simulations, including the zero-mobility trap states, is shown in Fig. 2).

the model, it has been proved that the electric switch is controlled by the energy transfer from the external bias to the charge carriers, which takes place when carriers occupy mobile states. Specifically, the simulative approach shows that, near threshold, carrier heating gives rise to a positive feedback: energy transfer from the field favors the occupation of the mobile states, which, in turn, increases the conduction of the material and, therefore, the energy transfer from the field. This determines the OTS transition to the low-resistivity, still-amorphous, phase.¹⁰ In view of these results, it is expected that the inclusion of mobile band-tail states into the physical model can significantly contribute to the heating process, thus influencing the electric switch.

In preliminary simulations of the amorphous phase,¹² we included the band-tail states as a single level E_U .

In the present work, the band-tail states are modeled by means of a more accurate energy spectrum, to obtain a quantitative indication of their impact on OTS. The $I(V)$ characteristic and the dynamics of the heating process are studied for nanometer-size structures, which is the present scientific and technological challenge;^{13–15} the sensitivity of the results with respect to a number of parameters, characteristic of the band-tail states (namely, their energy distribution, density, and mobility), is also investigated. The paper is organized as follows: Section II describes the physical model and lists the parameters used in the simulations; Sec. III shows the numerical scheme used to solve the model equations; Sec. IV illustrates the results and analyses the sensitivity of the threshold voltage on the parameters describing the band-tail states; finally, conclusions are drawn in Sec. V.

II. THE MODEL

The structure of the energy states of the material is sketched in Fig. 2; the figure reports only the energies deriving from the material structure: the calculation of the Fermi level, which is determined by the carrier population, is outlined later (Sec. II D). The band structure of Fig. 2 refers to a test case, without considering any specific chalcogenide. A unipolar conduction is assumed, carried by electrons; a suitable reversal of the band structure makes the modeling of a *p*-type material possible.

Considering the amorphous phase, we describe the trap states as concentrated in a thin interval of energies centered on a value E_T (Fig. 2). The trap states have a vanishing mobility, $\mu_T = 0$, and a volume concentration per unit energy $g_T(E)$.

The conduction band is modeled using a parabolic dispersion; its lower edge is indicated with E_C , and the distance of the latter from the trap states is $\Delta = E_C - E_T$. The density of states per unit energy and the mobility of the conduction band are $g_B(E)$ and $\mu_B = \text{const}$, respectively.

Finally, let E_{U1} and E_{U2} be the lower and upper edges of the band-tail states of the conduction band, with $g_U = \text{const}$ and $\mu_U = \text{const}$ being the corresponding density of states per unit energy and mobility, respectively. It must be noted that the actual form of the density of states g_U is such that the number of states is larger near the edge of the conduction band and smaller away from it. Approximating g_U with a constant implies that the simulations capture the average effect of the band-tail states; the calculations have been repeated using different positions of the lower edge of

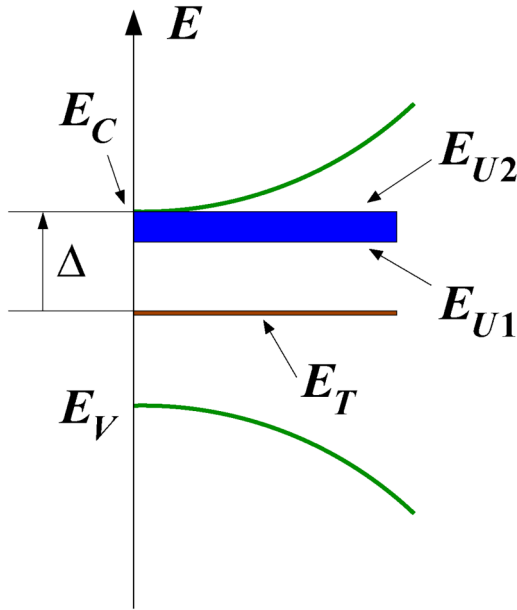


FIG. 2. Band structure of the chalcogenide material adopted in the present simulations, with the band-tail states modeled as a band extending from E_{U1} to E_{U2} . The trap energies are centered on $E_T = 0$, and the conduction band is modeled using a parabolic dispersion.

the tail. The upper edge E_{U2} is fixed and is assumed to coincide with the lower edge E_C of the conduction band. As mentioned above, the lower edge E_{U1} will take different values in the simulations; in all cases, it fulfills the prescription $E_{U1} > E_T$.

In the calculations carried out throughout this paper, the zero of energy is taken at E_T , so that $E_C = E_{U2} = \Delta$. The issue of the constancy of μ_U is discussed in Sec. IV with reference to Fig. 4.

The concentrations of the carriers in the trap states, in the band-tail states, and in the conduction band are n_T , n_U , and n_B , respectively; their sum at equilibrium is $n_{T0} + n_{U0} + n_{B0} = n_0$, neutralized by an equal concentration of charges of the opposite sign (the lists of symbols, units, and ranges of the parameters are given in Tables I, II, and III). The transport model is of hydrodynamic type, supplemented with a trap-limited transport, namely, field-assisted (Poole) transitions between localized and mobile states (the details of the model are given below). In contrast to the Monte Carlo method, in which the individual flights of the carriers are analyzed, the hydrodynamic model considers the behavior of the carrier populations averaged by distribution functions; such populations are influenced by carrier-carrier and carrier-phonon interactions and by the absorption of energy from the applied electric field. At equilibrium, the carriers are distributed over the T , U , and B states according to the Fermi distribution. In a non-equilibrium condition, the actual distributions are supposed to tend to Fermi-like forms with a local temperature T_e and quasi-Fermi level E_F ; these forms, here named *tendential distributions*, are determined in terms of T_e and E_F , which, in turn, are self-consistently evaluated from the model equations (see

TABLE I. Parameter symbols.

Parameter	Symbol
Fermi level	E_{F0}
Quasi-Fermi level	E_F
Energy level of the traps (fixed to zero)	E_T
Conduction-band edge	E_C
$E_C - E_T$	Δ
Lower energy of the band-tail states	E_{U1}
Upper energy of the band-tail states	E_{U2}
Concentration of trap states	G_T
Concentration of trap states per unit energy	g_T
Concentration of band-tail states	G_U
Concentration of band-tail states per unit energy	g_U
Concentration of band states per unit energy	g_B
Carrier concentration of the trap states	n_T
Carrier concentration of the band-tail states	n_U
Carrier concentration of the band states	n_B
Total carrier concentration at equilibrium	n_0
Band-carrier effective mass relative to m_0	m^*
Energy density of the trap carriers	\mathcal{E}_T
Energy density of the band-tail carriers	\mathcal{E}_U
Energy density of the band carriers	\mathcal{E}_B
Energy flux of the band-tail carriers	σ_U
Energy flux of the band carriers	σ_B
Mobility of the carriers in the band-tail states	μ_U
Mobility of the band carriers	μ_B
Poole coefficient	γ
Relaxation time of the carrier concentration	τ_n
Temperature-relaxation time of the trap carriers	τ_{TT}
Temperature-relaxation time of the band-tail carriers	τ_{TU}
Temperature-relaxation time of the band carriers	τ_{TB}

Secs. II A, II B, and II C). It must be specified that the tendential distribution is not the actual state of the carrier distribution; the individual concentrations and energies of the band, band-tail states, and traps, are obtained by solving the model of Secs. II E and II F. The tendential distribution is the Fermi distribution that the carriers would assume with the quasi-Fermi level E_F and non-equilibrium

TABLE II. Parameters kept fixed in the simulations.

Symbol	Units	Value
Δ	eV	0.35
n_0	m^{-3}	6.8×10^{25}
m^*	—	1
E_{U2}	eV	Δ
G_T	m^{-3}	$2 \times n_0$
μ_B	$\text{m}^2 \text{V}^{-1} \text{s}^{-1}$	4×10^{-4}
γ	C m	5×10^{-28}
τ_n	ps	0.5
τ_{TT}	ps	100
τ_{TU}	ps	1.8
τ_{TB}	ps	1.0

20 September 2024 09:29:02

TABLE III. Parameters of the band-tail states changed during the simulations. The minimum and maximum values are defined with respect to the standard values listed in Eq. (16).

Symbol	Units	Min.	Max.
E_{U1}	eV	0.2Δ	0.8Δ
G_U	m^{-3}	0.5×10^{25}	10^{25}
μ_U	$\text{m}^2 \text{V}^{-1} \text{s}^{-1}$	2×10^{-5}	6×10^{-5}

temperature T_e compatible with their global concentration and energy. Being it a collective phenomenon, the relaxation time of the tendential distribution is the same for all populations.

A. Band states

Considering the band states first, from the definitions given in Sec. II, it follows for the tendential band concentration

$$\tilde{n}_B = \int_{\Delta}^{\infty} \frac{g_B(E) dE}{1 + \exp[(E - E_F)/(k_B T_e)]}, \quad (1)$$

with T_e being the local temperature and E_F being the local quasi-Fermi level of the carriers. It is assumed that $\Delta - E_F \gg k_B T_e$; in turn, a parabolic band is considered, with m^* being the effective mass. Equation (1) then becomes

$$\tilde{n}_B \simeq g_B(T_e) \exp\left(\frac{E_F - \Delta}{k_B T_e}\right), \quad g_B = \left(\frac{m^* k_B T_e}{2^{1/3} \pi \hbar^2}\right)^{3/2}. \quad (2)$$

The tendential energy per unit volume of the band carriers, $\tilde{\epsilon}_B$, is found from (1) by the replacement $g_B(E) \leftarrow E g_B(E)$ in the integrand; using the same approximation as above yields

$$\tilde{\epsilon}_B \simeq \left(\Delta + \frac{3}{2} k_B T_e\right) g_B(T_e) \exp\left(\frac{E_F - \Delta}{k_B T_e}\right). \quad (3)$$

The equilibrium concentration n_{B0} and energy density ϵ_{B0} of the band carriers are described by expressions of the forms (1) and (3) with replacements $T_e \leftarrow T_0$ and $E_F \leftarrow E_{F0}$, with T_0 being the equilibrium lattice temperature and E_{F0} being the Fermi level; it is implied that the condition $\Delta - E_{F0} \gg k_B T_0$ holds. Also, since the Poole effect is considered in the simulation, one must replace Δ with $\Delta' = \Delta - \gamma |F|$.

B. Band-tail carriers

Assuming $E_{U1} - E_F \gg k_B T_e$ and remembering that $g_U = \text{const}$, the tendential concentration of the carriers in the band-tail states is given by

$$\begin{aligned} \tilde{n}_U &= \int_{E_{U1}}^{\Delta} \frac{g_U dE}{1 + \exp[(E - E_F)/(k_B T_e)]} \\ &\simeq g_U k_B T_e \left[\exp\left(-\frac{E_{U1} - E_F}{k_B T_e}\right) - \exp\left(-\frac{\Delta - E_F}{k_B T_e}\right) \right]. \end{aligned} \quad (4)$$

Similarly, the tendential energy per unit volume of the band-tail carriers is expressed as

$$\tilde{\epsilon}_U = g_U k_B T_e \left[\frac{E_{U1} + k_B T_e}{\exp[(E_{U1} - E_F)/(k_B T_e)]} - \frac{\Delta + k_B T_e}{\exp[(\Delta - E_F)/(k_B T_e)]} \right]. \quad (5)$$

In contrast to Sec. II A, in Eqs. (4) and (5), the replacement $\Delta \leftarrow \Delta' = \Delta - \gamma |F|$ is not done because here the Poole effect is assumed to be ineffective; in fact, when a carrier makes a transition into a band-tail state it may move only through hopping and cannot absorb from the electric field the energy necessary for the transition.

The equilibrium values are obtained from Eqs. (4) and (5) by letting $T_e \leftarrow T_0$ and $E_F \leftarrow E_{F0}$.

C. Trapped carriers

When the trap states are considered, the approximation of neglecting the unity in the denominator of the Fermi statistics is not applicable because the Fermi (or quasi-Fermi) level may be close to the trap level. On the other hand, remembering that the traps are concentrated in a thin interval of energies around $E_T = 0$, to the purpose of calculating the tendential concentration and energy, one approximates the density of states per unit volume as $g_T(E) \simeq G_T \delta(E - E_T)$, with $G_T = \text{const}$, to find

$$\tilde{n}_T = \frac{G_T}{1 + \exp[(E_T - E_F)/(k_B T_e)]}, \quad \tilde{\epsilon}_T = 0. \quad (6)$$

Again, the equilibrium concentration is found by letting $T_e \leftarrow T_0$ and $E_F \leftarrow E_{F0}$ in the first of Eq. (6).

D. Initial condition and Fermi level

As detailed in Sec. III, the numerical solution is carried out by the forward Euler scheme, starting from equilibrium (no applied voltage). The initial condition consists in prescribing the equilibrium temperature T_0 and the equilibrium, spatially uniform total carrier concentration $n_{B0} + n_{U0} + n_{T0} = n_0$, this leaving the Fermi level E_{F0} as the only unknown; the latter equality provides an algebraic equation in the unknown $\exp[-E_{F0}/(k_B T_0)]$. From this, E_{F0} is readily found, and the individual summands n_{B0} , n_{U0} , and n_{T0} are calculated from the equilibrium form of Eqs. (2) and (4) and of the first of Eq. (6), respectively. In turn, the total energy at equilibrium reads

$$\epsilon_{\text{tot}}^{\text{eq}} = \epsilon_{B0} + \epsilon_{U0} + \epsilon_{T0}, \quad (7)$$

where the first two summands are obtained as the equilibrium limits of Eqs. (3) and (5), respectively, and $\epsilon_{T0} = 0$.

E. Continuity equations

Letting j_B indicate the flux of the band carriers, it is expected that $\partial n_B / \partial t + \partial j_B / \partial x \neq 0$, because in a non-equilibrium condition, these carriers redistribute themselves among the band states, band-tail states, and trap states. The reasoning applies also to the n_U and n_T concentrations so that the continuity equations for n_T ,

n_U , and n_B , in the relaxation-time approximation read

$$\frac{\partial n_{T,U,B}}{\partial t} + \frac{\partial j_{T,U,B}}{\partial x} = -\frac{n_{T,U,B} - \tilde{n}_{T,U,B}}{\tau_n}, \quad (8)$$

with $\tilde{n}_{T,U,B}$ being the tendential concentrations defined above and τ_n being the relaxation time of the carrier concentrations. From $\mu_T = 0$, it follows that one must let $j_T = 0$ when considering the equation for the carriers in the traps. The relaxation time of the recombination, τ_n , whose value is given in Table II, is the same in the three equations (8); this is justified by observing that it must be $n_T + n_U + n_B = \tilde{n}_T + \tilde{n}_U + \tilde{n}_B$ identically, and that, when the three equations (8) are added up, the sum of the left hand sides vanishes.

As for the continuity of energy, let ε_{tot} be the total energy per unit volume of the carriers. The energy fluxes in the band-tail states and band states are given by, respectively,

$$\sigma_U = \frac{\tilde{\varepsilon}_U}{\tilde{n}_U} j_U, \quad \sigma_B = \left(\Delta + \frac{3}{2} k_B T_e \right) j_B, \quad (9)$$

with \tilde{n}_U given by (4) and $\tilde{\varepsilon}_U$ given by (5). The above expressions have been obtained assuming that the average carrier energy can be approximated with the corresponding tendential values; this approximation is applicable if the variation in the external voltage is very slow with respect to the relaxation times of the system (see below). The energy flux of the trap states is zero since $j_T = 0$. As before, it is expected that $\partial \varepsilon_{\text{tot}} / \partial t + \partial(\sigma_U + \sigma_B) / \partial x \neq 0$ because in a non-equilibrium condition the carriers exchange energy with the electric field F and, at the same time, their energy relaxes to the phonon bath; thus,

$$\frac{\partial \varepsilon_{\text{tot}}}{\partial t} + \frac{\partial(\sigma_U + \sigma_B)}{\partial x} = (j_U + j_B) q F - \left(\frac{\partial \varepsilon_{\text{tot}}}{\partial t} \right)_{\text{ph}}. \quad (10)$$

In Eq. (10), term

$$\left(\frac{\partial \varepsilon_{\text{tot}}}{\partial t} \right)_{\text{ph}} = \left(\frac{\partial \varepsilon_T}{\partial t} \right)_{\text{ph}} + \left(\frac{\partial \varepsilon_U}{\partial t} \right)_{\text{ph}} + \left(\frac{\partial \varepsilon_B}{\partial t} \right)_{\text{ph}} \quad (11)$$

represents the time variation in the total energy density due to the interaction with phonons, that is, the energy relaxation of T -, U -, and B -carriers to the thermal bath (the latter is supposed to be at equilibrium at every time). Furthermore, since the three types of carriers share the same quasi-Fermi level E_F and non-equilibrium temperature T_e , the latter is assumed to be representative of the common average tendential energy; consequently, in the relaxation-time approximation,

$$\left(\frac{\partial \varepsilon_X}{\partial t} \right)_{\text{ph}} \simeq n_X \frac{k_B (T_e - T_0)}{\tau_{TX}}, \quad (12)$$

where X stands for T , U , or B .

F. Transport equations and Poisson equations

The transport equations for the band and the localized states are of the drift-diffusion form,

$$j_{U,B} = \mu_{U,B} n_{U,B} F - \frac{\partial(Dn)_{U,B}}{\partial x}, \quad j_T = 0, \quad (13)$$

with

$$D_B = \frac{k_B T_e}{q} \mu_B, \quad D_U = \frac{k_B T_e}{q} \mu_U. \quad (14)$$

The model is completed by the Poisson equation

$$\frac{\partial F}{\partial x} = \frac{q}{\varepsilon_a} (n_T + n_U + n_B - n_0), \quad (15)$$

with ε_a being the permittivity of the material. As mentioned above, at equilibrium, the local charge neutrality is fulfilled, $n_{B0} + n_{U0} + n_{T0} - n_0 = 0$, and the applied voltage V is zero so that $F = 0$ everywhere. In the non-equilibrium condition, neither the local nor the global charge neutrality of the chalcogenide region is fulfilled. The two metal contacts at the ends of the device are assumed ideal so that the interior of each metal region is equipotential. In the non-equilibrium condition, the contacts keep the charge neutrality at $x = 0$ and $x = L$, and a charge layer forms at each metal-chalcogenide interface on the metal side of the interface; the two layers, together with the non-zero global charge inside the chalcogenide, keep the global neutrality of the whole structure.

Equations (8), (10), (13), and (15) form a system of seven equations. As shown in paragraphs II A, II B, and II C, the tendential concentrations and energy densities are expressible in terms of the non-equilibrium temperature T_e and quasi-Fermi energy E_F ; therefore, the unknowns of the system are also seven, specifically, n_T , n_U , n_B , ε_{tot} , F , T_e , and E_F .

III. NUMERICAL SOLUTION

Equations (8), (10), (13), and (15) were solved with the forward Euler method, in which the complicity of the model dictated a small integration step ($\Delta t = 10^{-16}$ s).

The applied voltage V is updated at the end of each time step. Like in the equilibrium case, from the last available value of T_e , one determines E_F by solving an algebraic equation; then, from T_e and E_F , one obtains the tendential concentrations and energies. Finally, solving Eqs. (8), (10), (13), and (15) yields the updated values of the unknowns.

No numerical instability was detected during the simulations; an accuracy of about 10% is considered appropriate to compare the simulations with the experimental data.

To identify the influence of the band-tail states, a number of simulations have been carried out using the model described in Sec. II. Apart from those describing the band-tail states, the model parameters have been fixed to the values listed in Table II; as for the band-tail states, their parameters have been given different values inside the ranges specified in Table III: such values were chosen as to keep the validity of Eqs. (4) and (5). As anticipated in the caption of the same table, a set of standard values have also

been identified for these parameters; they are

$$\begin{cases} E_{U1} = 0.4\Delta & \text{eV} \\ G_U = 10^{25} & \text{m}^{-3} \\ \mu_U = 4 \times 10^{-5} & \text{m}^2 \text{V}^{-1} \text{s}^{-1}. \end{cases} \quad (16)$$

IV. RESULTS

A first batch of simulations have been carried out to check the influence of the band-tail states: Fig. 3 shows the total carrier flux as a function of the average electric field V/L (where V is the applied voltage and $L = 20 \text{ nm}$ is the device length), with and without the presence of band-tail states (the standard parameters were used in the former case). The main result to be noted is a reduction of the threshold field, due to the contribution of the band-tail states. The effect is detailed in Fig. 4, where the different contributions to the total flux when the band-tail states are present are shown. The figure shows that the carrier flux is dominated by the band-tail states at low and intermediate fields: these states are in fact characterized by energies easily accessible by carriers belonging to the localized trap states of the gap. At high fields, the band states are increasingly populated and produce the heating process that eventually brings to the sudden increase in conduction that sets in at the threshold field. The dominance of the band flux at high fields justifies the approximation of considering a constant mobility μ_U of the band-tail states. In fact, μ_U increases with T_e ; on the other hand, below threshold, T_e is close to the equilibrium value T_0 so that the influence of the carrier temperature on μ_U takes place when the contribution of the band-tail states to the total flux is not relevant any more.

Figure 5 shows the non-equilibrium carrier temperature T_e vs. the average electric field, again in the two cases where the band-tail states are present or absent. The presence of band-tail states favors the carrier-heating process determining the decrease of the threshold field observed in Figs. 3 and 4.

Figure 6 shows the carrier concentrations of the traps, band-tail states, and conduction band vs. the average electric field, still using the standard parameters for the band-tail states. Consistently with the outcome of Fig. 4, the carrier concentration of the band states increases when the field increases; the carrier concentration

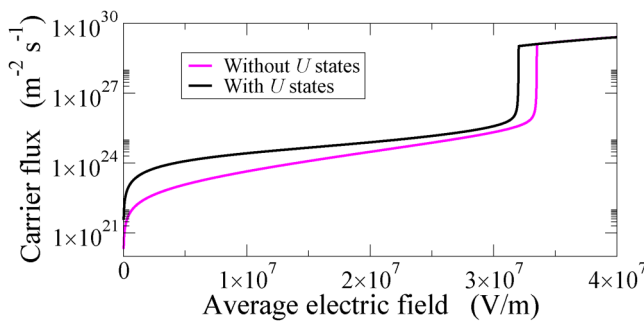


FIG. 3. Total carrier flux j_{tot} vs. the average electric field V/L , with and without the presence of band-tail states (see text).

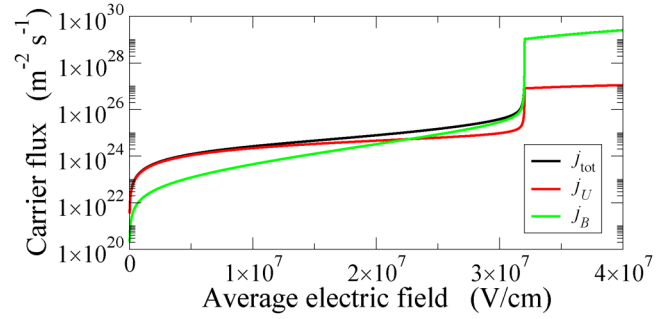


FIG. 4. Total carrier flux j_{tot} , carrier flux j_U of the band-tail states, and carrier flux j_B of the conduction band vs. the average electric field V/L (see text).

in the band-tail states, instead, is almost insensitive to the field increase, being the band-tail states populated from trap states even in near-equilibrium conditions.

The next batch of simulations analyze the effects of variations in the band-tail parameters with respect to the standard values; the effect of varying the energy range of the band-tail states is analyzed in Figs. 7–11. Figures 7 and 8 refer to the carrier flux obtained by varying the lower edge E_{U1} of the band-tail states. Besides the standard value $E_{U1} = 0.4\Delta$, the values $E_{U1} = 0.2\Delta$ (Fig. 7) and $E_{U1} = 0.8\Delta$ (Fig. 8) have been tested.

By the same token, the effects of a change in E_{U1} on the carrier concentrations have been tested as well (Figs. 9 and 10). Clearly, when the edge of the band-tail states gets closer to the trap states ($E_{U1} = 0.2\Delta$), the population of the band-tail states dominates the carrier flux in a larger range of electric fields. Furthermore, the increased number of carriers in states with nonzero mobility makes the carriers to populate the band states with higher efficiency and triggers a substantial decrease in the threshold field. The opposite effect is obtained by shrinking the band tail toward the conduction-band edge ($E_{U1} = 0.8\Delta$): in this case, the heating process is slowed by a less effective carrier transfer from trap to band-tail states, with a consequent increase in the threshold field with respect to the reference set of parameters.

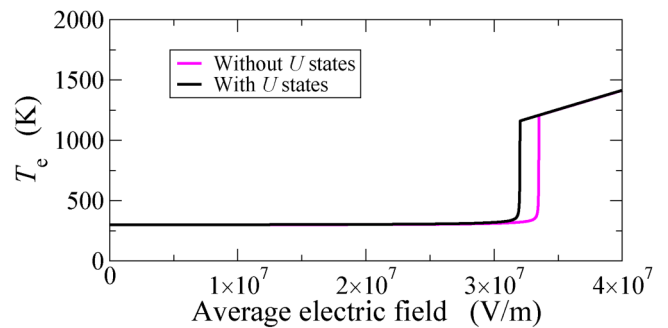


FIG. 5. Non-equilibrium carrier temperature T_e vs. the average electric field V/L , with and without the presence of band-tail states (see text).

20 September 2024, 09:29:02

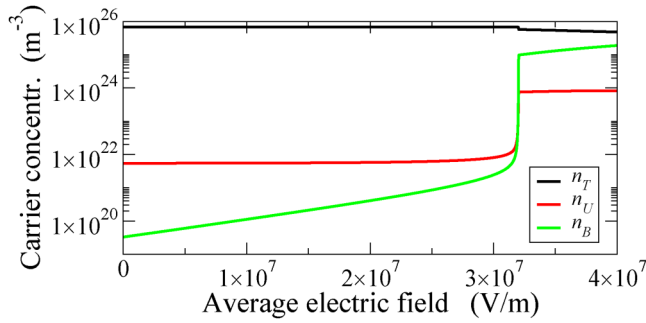


FIG. 6. Carrier concentration n_T of the traps, carrier concentration n_U of the band-tail states, and carrier concentration n_B of the conduction band vs. the average electric field V/L (see text).

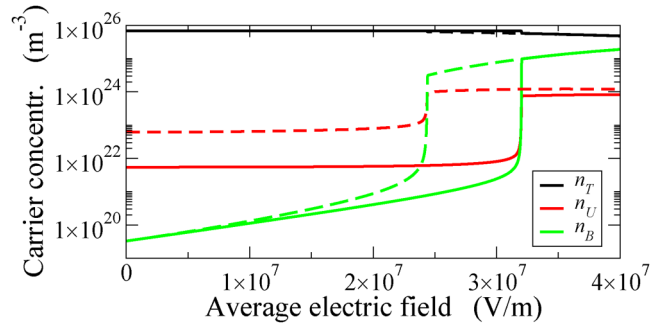


FIG. 9. Carrier concentration n_T of the traps, carrier concentration n_U of the band-tail states, and carrier concentration n_B of the conduction band vs. the average electric field V/L . The continuous lines are the same as in Fig. 6. The dashed lines show the variation in the corresponding concentrations when the lower edge E_{U1} of the band-tail states is brought from 0.4Δ to 0.2Δ . The other parameters were left unchanged.

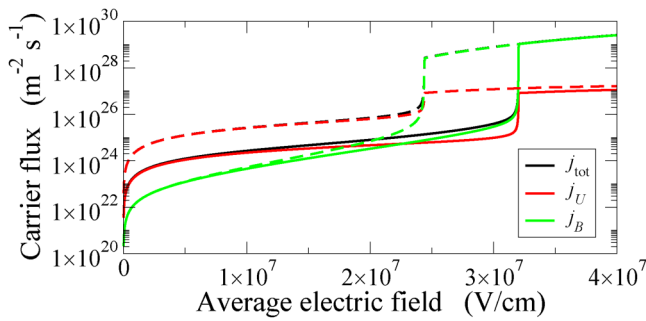


FIG. 7. Total carrier flux j_{tot} , carrier flux j_U of the band-tail states, and carrier flux j_B of the conduction band vs. the average electric field V/L . The continuous lines are the same as in Fig. 4. The dashed lines show the variation in the corresponding fluxes when the lower edge E_{U1} of the band-tail states is brought from 0.4Δ to 0.2Δ . The other parameters were left unchanged.

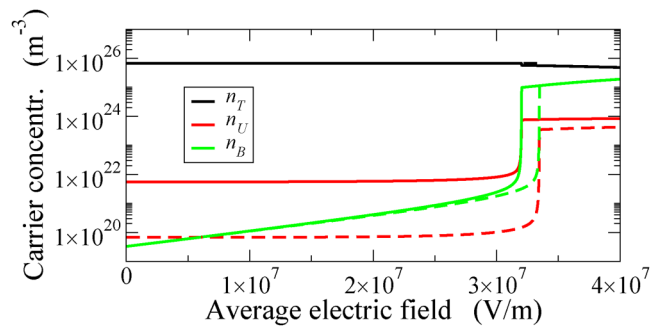


FIG. 10. Carrier concentration n_T of the traps, carrier concentration n_U of the band-tail states, and carrier concentration n_B of the conduction band vs. the average electric field V/L . The continuous lines are the same as in Fig. 6. The dashed lines show the variation in the corresponding concentrations when the lower edge E_{U1} of the band-tail states is brought from 0.4Δ to 0.8Δ . The other parameters were left unchanged.

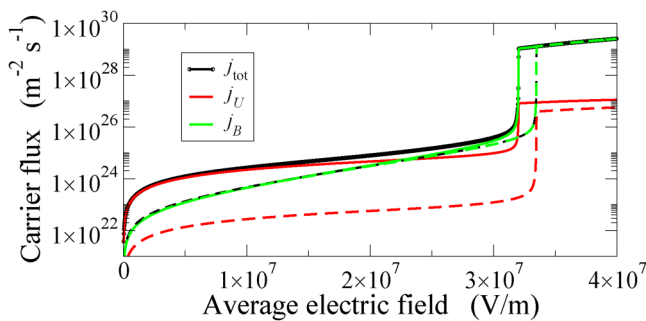


FIG. 8. Total carrier flux j_{tot} , carrier flux j_U of the band-tail states, and carrier flux j_B of the conduction band vs. the average electric field V/L . The continuous lines are the same as in Fig. 4. The dashed lines show the variation in the corresponding fluxes when the lower edge E_{U1} of the band-tail states is brought from 0.4Δ to 0.8Δ . The other parameters were left unchanged.

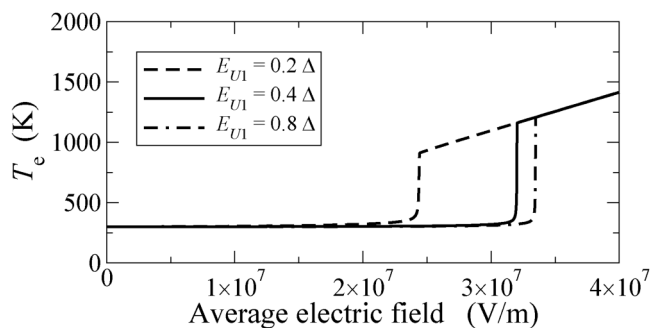


FIG. 11. Non-equilibrium carrier temperature T_e vs. the average electric field V/L , corresponding to different values of the lower edge E_{U1} of the band-tail states (see the inset).

20 September 2024, 09:29:02

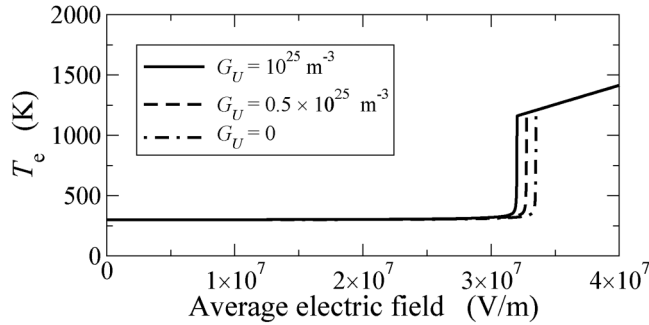


FIG. 12. Non-equilibrium carrier temperature T_e vs. the average electric field V/L , corresponding to different concentrations G_U of the band-tail states (see the inset).

The above interpretation is confirmed by analyzing the dependence of the carrier temperature on the average electric field, reported in Fig. 11 for the three values of E_{U1} considered here. It is apparent that the stronger effect on the onset of the OTS switch is obtained by reducing the gap between localized and band-tail states: even if the latter have a reduced mobility, nevertheless they contribute to carrier heating and, together, bridge the carrier transfer to the band states. When E_{U1} is equal to or above 0.4Δ , a reduced effect of the threshold field is predicted by our model.

The variation in the concentration of the band-tail states per unit energy (see Table III) brings a small effect on the threshold field, as shown in Fig. 12; this indicates that the band-tail states present in the gap play their bridging role even if their number is low. The same result is obtained by varying the mobility of the band-tail states up to two orders of magnitude (Figs. 13, 14, 15, and 16). The increase in mobility accelerates the heating, but the quantitative effect is not relevant; in turn, a decrease in mobility makes the fluxes to decrease and the threshold field to increase until, at very small mobilities, the threshold field tends to saturate.

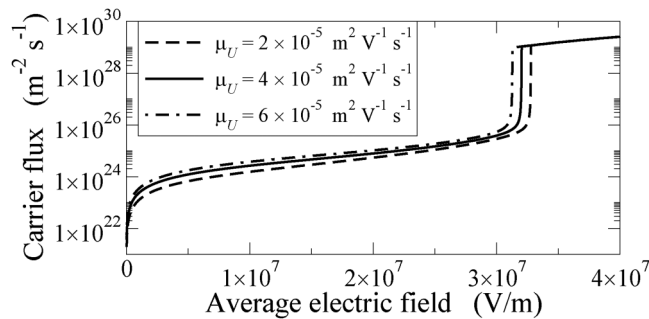


FIG. 13. Total carrier flux j_{tot} vs. the average electric field V/L , corresponding to different mobilities μ_U of the band-tail carriers (see the inset).

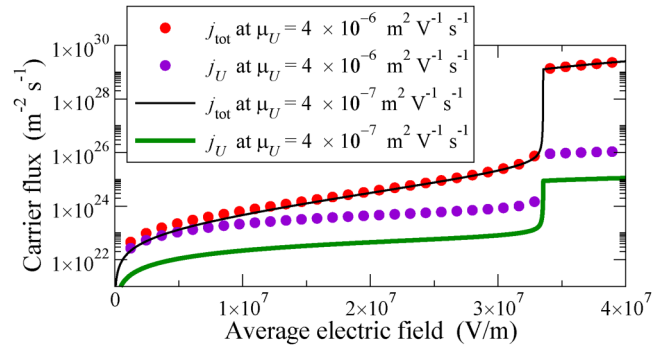


FIG. 14. The carrier flux calculated using much smaller values of μ_U (see the inset) with respect to the case of Fig. 13. As expected, the fluxes decrease and the threshold field slightly increases.

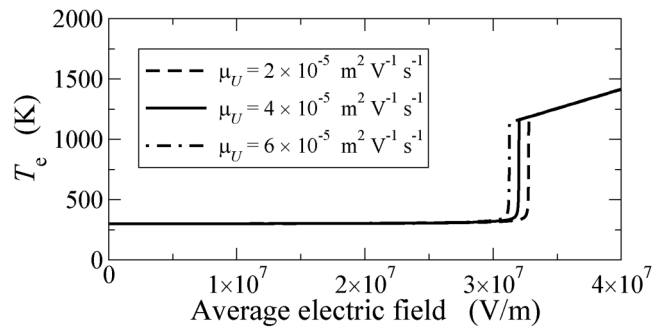


FIG. 15. Non-equilibrium carrier temperature T_e vs. the average electric field V/L , corresponding to different mobilities μ_U of the band-tail carriers (see the inset).

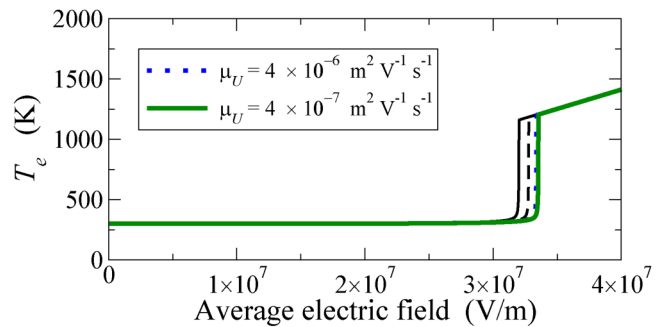


FIG. 16. With reference to the vertical portions of the graph, the two leftmost curves replicate those of Fig. 15 corresponding to $\mu_U = 4 \times 10^{-5}$ and $\mu_U = 2 \times 10^{-5} \text{ m}^2 \text{ V}^{-1} \text{ s}^{-1}$. The other two curves are calculated using much smaller values of μ_U (see the inset), showing that the threshold field tends to saturate when μ_U decreases.

20 September 2024, 09:29:02

V. CONCLUSIONS

A hydrodynamic-like transport model for amorphous chalcogenides has been used to test the effect of band-tail states on the Ovonic switch of amorphous chalcogenides. The model has been solved by means of a robust and computationally efficient numerical procedure, suitable for design purposes. A test case has been considered in the calculations. The effects of the three relevant parameters characterizing the band-tail states, namely, the position of the lower edge of the tail, the density of states, and mobility, have been analyzed in order to provide guidelines to benchmark chalcogenide materials for specific applications. As a general trend, the band-tail states are populated by the large number of carriers transiting from the trap states; being mobile, they contribute to the flux and increase the power transferred by the field. Therefore, they favor the carrier transfer to the extended band states, thus anticipating the OTS switch.

As for their possible technological relevance, the effect on the $I(V)$ curves is weak as long as the lower edge of the band-tail states is sufficiently distant from the trap states. When it gets closer, instead, a significant lowering of the threshold field is detected: the energy flux due to carriers populating the band-tail states is dominant below, and up to, the OTS threshold and competes with the contribution coming from band states. It is, therefore, of utmost importance to pursue more detailed experimental or *ab initio* analyses of the density of states in the region of the energy gap of chalcogenide materials, in order to allow for a careful modeling of the OTS field.

ACKNOWLEDGMENTS

We wish to acknowledge fruitful discussions with Dr. Enrico Piccinini of Applied Materials Italia s.r.l. and with Dr. Arrigo Calzolari of the *Istituto Nanoscienze* of Consiglio Nazionale delle Ricerche.

AUTHOR DECLARATIONS

Conflict of Interest

The authors have no conflicts to disclose.

Author Contributions

R. Brunetti: Conceptualization (equal); Data curation (equal); Formal analysis (equal); Investigation (equal); Methodology (equal); Software (equal); Supervision (equal); Validation (equal); Writing – original draft (equal); Writing – review & editing (equal). **C. Jacoboni:** Conceptualization (equal); Data curation (equal); Formal analysis (equal); Investigation (equal); Methodology (equal); Software (equal); Supervision (equal); Validation (equal); Writing – original draft (equal); Writing – review & editing (equal). **M. Rudan:** Conceptualization (equal);

Data curation (equal); Formal analysis (equal); Investigation (equal); Methodology (equal); Software (equal); Supervision (equal); Validation (equal); Writing – original draft (equal); Writing – review & editing (equal).

DATA AVAILABILITY

The data that support the findings of this study are available from the corresponding author upon reasonable request

REFERENCES

- ¹A. Redaelli, *Phase Change Memory* (Springer, 2019).
- ²S. Raoux and M. Wuttig, *Phase Change Material—Science and Applications* (Springer, 2009).
- ³S. R. Ovshinsky, “Reversible electrical switching phenomena in disordered structures,” *Phys. Rev. Lett.* **21**, 1450 (1968).
- ⁴M. Anbarasu, M. Wimmer, G. Bruns, M. Salinga, and M. Wuttig, “Nano-second threshold switching of GeTe₆ cells and their potential as selector devices,” *Appl. Phys. Lett.* **100**, 143505 (2012).
- ⁵D. Kau, S. Tang, I. V. Karpov, R. Dodge, B. Klehn, J. A. Kalb, J. Strand, A. Diaz, N. Leung, J. Wu, S. Lee, T. Langtry, K. Chang, C. Papagianni, J. Lee, J. Hirst, S. Erra, S. Flores, N. Righos, H. Castro, and G. Spadini, “A stackable cross point phase change memory,” in *Proceedings of the International Electron Devices Meeting (IEDM)*, edited by V. Subramanian (IEEE, Baltimore, MD, 2009), pp. 617–620.
- ⁶F. Urbach, “The long-wavelength edge of photographic sensitivity and of the electronic absorption of solids,” *Phys. Rev.* **92**, 1324 (1953).
- ⁷N. Bacalis, E. N. Economou, and M. H. Cohen, “Simple derivation of exponential tails in the density of states,” *Phys. Rev. B* **37**, 2714–2717 (1988).
- ⁸S. Caravati, M. Bernasconi, T. D. Kühne, M. Krack, and M. Parrinello, “First-principles study of crystalline and amorphous Ge₂Sb₂Te₅ and the effects of stoichiometric defects,” *J. Phys.: Condens. Matter.* **21**, 255501 (2009).
- ⁹A. Cappelli, E. Piccinini, F. Xiong, H. Behnam, R. Brunetti, M. Rudan, E. Pop, and C. Jacoboni, “Conductive preferential paths of hot carriers in amorphous phase-change materials,” *Appl. Phys. Lett.* **103**, 083503 (2013).
- ¹⁰R. Brunetti, C. Jacoboni, E. Piccinini, and M. Rudan, “Band transport and localised states in modelling the electric switching of chalcogenide materials,” *J. Comp. Elect.* **19**, 128 (2020).
- ¹¹P. Fantini, N. Polino, A. Ghetti, and D. Ielmini, “Threshold switching by bipolar avalanche multiplication in ovonic chalcogenide glasses,” *Adv. Electron. Mater.* **9**, 2300037 (2023).
- ¹²R. Brunetti, C. Jacoboni, and M. Rudan, “Do Urbach tails matter in determining the electric properties of amorphous chalcogenides? A simulative approach to the problem,” in *22nd International Conference on Electron Dynamics in Semiconductors, Optoelectronics and Nanostructures (EDISON22)* (Münster, 2023), <https://www.uni-muenster.de/EDISON22/>
- ¹³M. Wimmer and M. Salinga, “The gradual nature of threshold switching,” *New J. Phys.* **16**, 113044 (2014).
- ¹⁴N. Saxena, R. Raghunathan, and A. Manivannan, “A scheme for enabling the ultimate speed of threshold switching in phase change memory devices,” *Sci. Rep.* **11**, 6111 (2021).
- ¹⁵R. Brunetti, C. Jacoboni, E. Piccinini, and M. Rudan, “Time-domain analysis of chalcogenide threshold switching: From ns to ps scale,” *Front. Phys.* **10**, 854393 (2022).